




Tailoring of spatial coherence in a multimode fiber by selectively exciting groups of eigenmodes

RUI MA,^{1,2}  HUA HUI ZHANG,¹ EGOR MANUYLOVICH,² SRIKANTH SUGAVANAM,²  HAN WU,³  WEI LI ZHANG,^{1,7}  VLADISLAV DVOYRIN,^{2,4} TAO PING HU,^{2,5} ZHI JIA HU,^{2,6}  YUN JIANG RAO,^{1,8} AND SERGEI K. TURITSYN^{2,4} 

¹Fiber Optics Research Centre, School of Information and Communication Engineering, University of Electronic Science & Technology of China, Chengdu 611731, China

²Aston Institute of Photonic Technologies, Aston University, Birmingham B4 7ET, United Kingdom

³College of Electronics and Information Engineering, Sichuan University, Chengdu 610064, China

⁴Aston-Novosibirsk Centre for Photonics, Novosibirsk State University, Novosibirsk, Russia

⁵College of Science, Nanjing Forestry University, Nanjing 210037, China

⁶School of Instrument Science and Opto-electronics Engineering, Hefei University of Technology, Hefei, Anhui 230009, China

⁷wl_zhang@uestc.edu.cn

⁸yjrao@uestc.edu.cn

Abstract: Control of the properties of speckle patterns produced by mutual interference of light waves is important for various applications of multimode optical fibers. It has been shown previously that a high signal-to-noise ratio in a multimode fiber can be achieved by preferential excitation of lower order spatial eigenmodes in optical fiber communication. Here we demonstrate that signal spatial coherence can be tailored by changing relative contributions of the lower and higher order multimode fiber eigenmodes for the research of speckle formation and spatial coherence. It is found that higher order spatial eigenmodes are more conducive to the final speckle formation. The minimum speckle contrast occurs in the lower order spatial eigenmodes dominated regime. This work paves the way for control and manipulation of the spatial coherence of light in a multimode fiber varying from partially coherent or totally incoherent light.

© 2020 Optical Society of America under the terms of the [OSA Open Access Publishing Agreement](#)

1. Introduction

Speckle phenomena play an important role in modern optics and various applications [1]. In laser speckle contrast imaging, speckle patterns are used to visualize tissue blood perfusion, or detect tiny surface changes [2–4]. However, in a conventional imaging system, speckle patterns generated by coherent light illumination greatly deteriorate the imaging quality and have to be suppressed as much as possible, leading to the so-called speckle-free imaging [5]. Usually, the capability of generating speckle is dependent on the coherence of the light source. Light with lower coherence produces a weaker speckle pattern when the beam is reflected or transmitted through a random medium. Therefore, speckle formation can be changed by controlling the coherence of light. A number of techniques have been proposed to generate partially coherent or totally incoherent light [6–8]. One of the attractive methods is to use a multimode fiber (MMF) since it supports hundreds of waveguide modes which could effectively reduce the spatial coherence when light is propagating through MMF [9–11].

MMFs are used in various practical applications such as optical communications, biological imaging, fiber sensing, high power lasers, and others. Recently, a great deal of attention was attracted to research on nonlinear effects, principal modes and image transmission in MMF

[12–16]. Typically, a strong modal interference induced speckle pattern is found at the output of MMF and its spatial coherence is also extensively studied [17–18]. To reduce the spatial coherence of light emitting from MMF, one should both increase the numerical aperture to enlarge the supported transverse mode number and use a sufficiently long MMF to achieve decoherence by efficient mixing of different waveguide modes [19,20].

It is known that light output from MMF has highly non-uniform modal weight distribution [21]. The modal weight distribution has an impact on spatial coherence and speckle formation. It is also shown that the higher order modes are more modal-noise sensitive in optical fiber communication due to their large transverse spatial frequencies [21–23]. However, different spatial modes are commonly treated equally when characterizing the spatial coherence of MMF based illumination light source [1,5]. Therefore, the problem of different contributions of lower and higher order modes to illumination beam coherence is of interest for the research area of designing individual fiber light source with customized spatial coherence.

In this work, we examine spatial coherence tailoring using selective excitation of different order spatial eigenmodes in MMF. In order to purely focus on the influence of different order spatial mode profiles on the speckle formation, mode composition within one plane is analyzed and the propagation induced modal phase is neglected. We analyze the speckle formation generated from the composited mode modulated by random phases. The modal weight distribution is approximated by a Gaussian distribution with adjusted parameters. It is found that lower and higher order spatial modes contribute unequally to the speckle formation, namely the higher order ones lead to higher speckle contrast. The minimum speckle contrast occurs in lower order spatial modes dominated regime. This work reveals the intrinsic origin of modal field dependent speckle pattern formation. We anticipate that our results will benefit the design of light sources for generation of partially coherent light using MMF.

2. Results and discussions

A low spatial coherence light source based on MMFs is attractive in applications such as speckle-free imaging. Here, to reveal the coherence characteristics of light emitted from the output of a MMF, we mainly focus on how individual modal power distribution of the MMF output facet affects the spatial coherence and its further illumination performance. In this way, guidance could be provided on what kind of modal power distribution should be excited to realize specified spatial coherence. First, different illumination light sources are simulated through changing modal composition on the output facet of the MMF. Spatial coherence is characterized through speckle contrast calculation numerically to reveal the relationship of modal composition and spatial coherence, i.e., the unequal contribution of lower and higher order modes to spatial coherence. In the last part, an experimental work is carried out to verify this modal composition dependent spatial coherence.

2.1. Mathematical simulation model

In an optical fiber any (normalized) arbitrary propagating field $U(u)$ can be projected on the transverse spatial eigenmodes $\psi_n(u)$ of the fiber, which can be expressed as:

$$U(u) = \sum_{n=1}^{n_{\max}} c_n \psi_n(u), \quad (1)$$

where u represents the transverse coordinates, n denotes the n^{th} order eigenmode of the fiber, c_n are the modal coefficients [24]. Due to the orthonormal property, different spatial eigenmodes

have the relationship as:

$$\langle \psi_n, \psi_m \rangle = \iint_{R^2} d^2u \psi_n^*(u) \psi_m(u) = \delta_{nm}. \quad (2)$$

The supported spatial eigenmodes of a fiber waveguide can be calculated using the finite difference method [25]. Detailed information on how to calculate the spatial eigenmodes of a specified waveguide structure could be found from the cited reference and the corresponding author's website [26]. It is worth noting that the calculated spatial eigenmodes here are theoretically supported spatial modes defined by the fiber structure, not the estimated or empirical linear polarized modes. In order to investigate a fiber with a large number of spatial eigenmodes, an extra-large mode area step-index MMF (the cross-section of the core is circular with core diameter of 104 μm and numerical aperture NA of 0.24) is mathematically analyzed. Figure 1(a) gives the lateral view of the fiber's refractive index profile. Only monochromatic light with a wavelength of 1550 nm is considered here. The calculated effective refractive index n_{eff} of the 500 spatial eigenmodes at the wavelength of 1550 nm is shown in Fig. 1(b). The spatial eigenmodes are numbered with the reduction of the n_{eff} . Electric field profiles of representative spatial eigenmodes and corresponding effective refractive index are shown in Fig. 2. From the electric field profiles of the above spatial eigenmodes, we can anticipate that different orders of modes couldn't be simply treated equally in the spatial decoherence process.

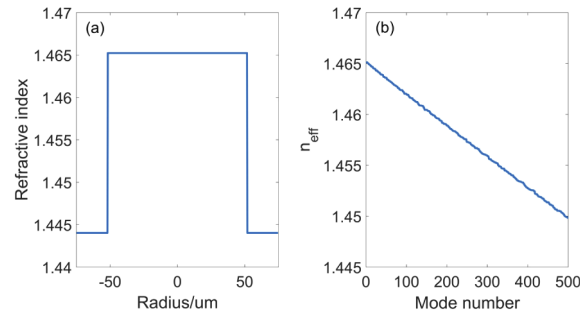


Fig. 1. (a) Lateral view of the fiber's refractive index profile. (b) Calculated effective refractive index of the 500 spatial eigenmodes.

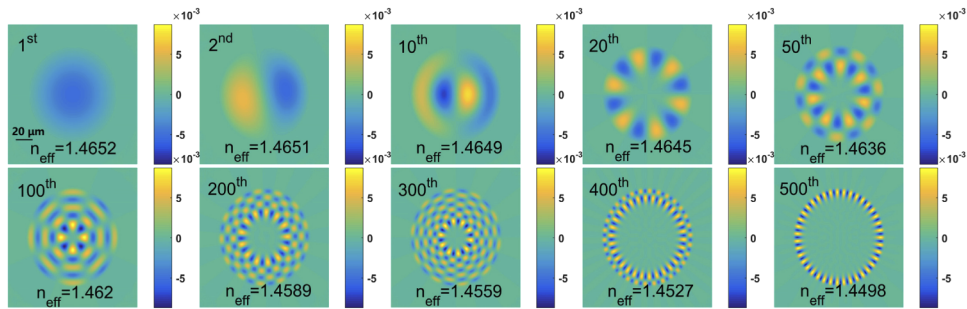


Fig. 2. Electric field profiles of representative spatial eigenmodes and corresponding effective refractive index. The color bar represents the amplitude of the electric field profiles with arbitrary unit.

The modal coefficients c_n are given by

$$c_n = \rho_n \exp(i\phi_n) = \langle \psi_n, U \rangle = \iint_{R^2} d^2u \psi_n^*(u) U(u), \quad (3)$$

where ρ_n and ϕ_n represent modal amplitude and phase respectively. The modal coefficients c_n are normalized by:

$$\sum |c_n|^2 = \sum |\rho_n|^2 = 1. \quad (4)$$

The modal field from the MMF is essentially the spatial interference pattern of all the considered spatial eigenmodes, which can be simulated by adding the eigenmode's electric fields with proper modal coefficients, as given by Eq. (1). In this way, the composition of the output field can be modulated by changing the values of c_n and different illumination scenarios based on MMF can be flexibly simulated.

In order to evaluate the effects of the interplay between the number of spatial eigenmodes and modal weight distribution (the $|c_n|^2$ distribution for all the considered spatial eigenmodes) on the spatial coherence from the MMF, five groups of total mode number ($M=100, 200, 300, 400$ and 500) have been considered. Figure 3 gives several examples of representative modal weight distributions with total mode number of 100 and 500. It is worth noting that the 100 modes in Fig. 3(a) correspond to the first lower order 100 spatial eigenmodes calculated in Fig. 1(b), while the 500 modes in Fig. 3(b) represent the total set of spatial eigenmodes. Here we assume that the modal weights follow the Gaussian distribution which is defined by mean value μ and standard deviation σ . Only half of the Gaussian curve is applied for the modal weight distribution. Therefore, the regimes dominated by lower order modes ($\mu = 0$) and higher order modes ($\mu = M$) are simulated separately. In this way, different modal weight distributions can be implemented by adjusting these two parameters. The integral of the modal weights for each distribution curve is set to be one to fulfill the normalization condition given by Eq. (4).

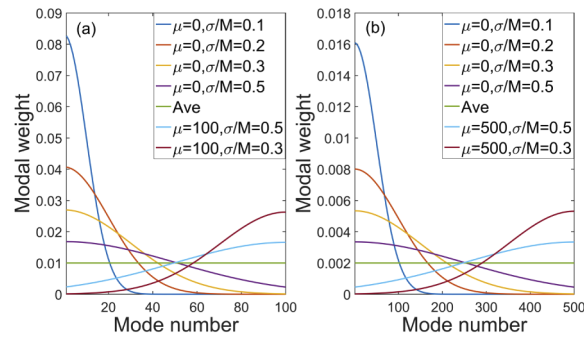


Fig. 3. Modal weight with different Gaussian distribution for total mode number of 100 (a) and 500 (b).

Taking the total mode number $M=100$ in Fig. 3(a) as an example, by setting the mean value $\mu=0$, we have the distribution when the lower order (the order number that is smaller than $M/2$) spatial eigenmodes always have larger modal weights than the higher order modes (the order number that is larger than $M/2$). By gradually increasing the ratio of σ/M , the modal weights keep transferring from lower order modes to higher order ones and the weight distribution gets more and more even, as shown in Fig. 3(a). The green line in Fig. 3 corresponds to a totally uniform distribution with equal power in all the modes. By setting the mean value $\mu = 100$, the higher order modes have more power than the lower order ones. In this regime, with the ratio of σ/M reducing, the modal weights still keep transferring from lower order modes to higher order ones. The tendency for the 500 total mode number group in Fig. 3(b) is similar, except for each individual value of σ/M there are more spatial eigenmodes than the 100 group. In this way, different modal weight distributions can be realized for further analysis.

2.2. Simulation results and discussions

Here, we only focus on the illumination from the output facet of the MMF and the speckle formation purely produced by different order spatial eigenmodes. Therefore, we neglect the propagation induced modal phase differences among different order spatial eigenmodes and set all the modal phase ϕ_n to be the same during the mode composition. Using the generated modal weight distributions, varying spatial intensity profiles from the output of MMF can be obtained, as shown in Fig. 4. From the calculated spatial intensity profile, strong interference induced laser speckle patterns are obviously observed. For each total mode number group, with the modal weight transferring from lower order to higher order modes, the speckle grains get much smaller and more notable within the fiber core region. This means that with the higher order modes getting higher fraction of power, they become effective modes and contribute more to the final interference induced laser speckle patterns. It is also shown that lower and higher order modes have dramatically different impacts. For example, for the same $\sigma/M=0.1$ value of the two regimes, $\mu=0$ (lower order modes dominated regime) and $\mu=M$ (higher order modes dominated regime), the latter one shows denser formed speckle grains. For each column, which represents different total mode number groups but with the same σ/M value, the lower row with 500 total mode number always shows much smaller grains, which means the speckle is more notable. Therefore, the modal weight distribution has a significant impact on the formation of the final spatial profile.

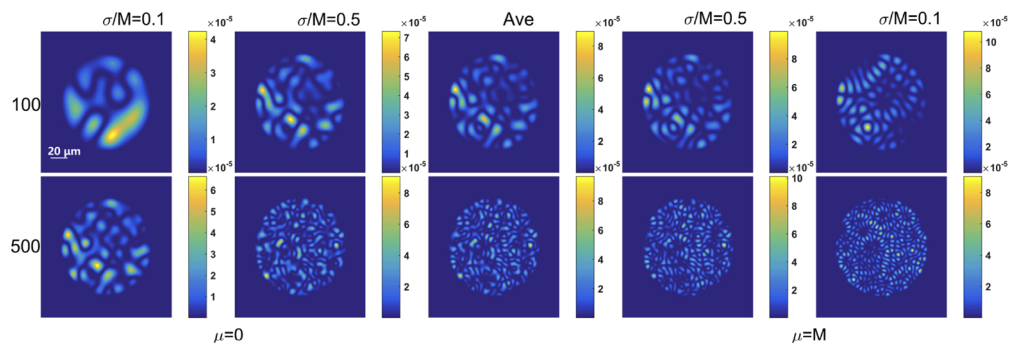


Fig. 4. Calculated spatial intensity profiles with different modal composition defined by σ/M for total mode number of 100 (the upper row) and 500 (the lower row). The modal weights keep transferring from the lower order eigenmodes to higher order eigenmodes from the left case to the right one for each row. The color bar represents intensity with arbitrary unit.

Spatial coherence from the MMF is usually measured through interferometry, like the Mach-Zehnder interferometer [17] or the Young's interferometer [27]. It can also be analyzed by light propagating through a random diffuser like ground glass to get a random phase modulation and therefore generates speckle pattern [5,11]. By calculating the speckle contrast value C from the speckle pattern (the speckle contrast C is defined by the relation $C = \sigma_I / \langle I \rangle$, where σ_I and $\langle I \rangle$ are the standard deviation of the intensity and the average intensity, respectively), one can not only get a rough evaluation of the spatial coherence, but also directly connect its illumination capability with individual imaging techniques, where a light source with specified speckle contrast is needed, such as speckle-free imaging (low speckle contrast), and laser speckle contrast analysis (high speckle contrast). Here, to investigate the speckle pattern formation, we modulate each weighted mode from the MMF with a random phase matrix with values uniformly distributed over $[-\pi, \pi]$. The random phase is imposed on each order of spatial eigenmodes through similar technique used in mode division multiplexing [28], i.e. the random phase modulation is imposed in Fourier domain and all the obtained speckle patterns are composed together afterward. It is worth noting that by applying this random phase modulation to the composite mode, it would

eliminate the role of modal phase ϕ_n , even if we considered modal phase ϕ_n during the modal composition part. Therefore, each weighted spatial eigenmodes would generate an individual diffracted speckle pattern after the random phase modulating process. Then all these speckle patterns are composed together to generate the whole speckle pattern for this individual modal weight distribution, as shown in Fig. 5. It can be seen that for each value of σ/M , the lower row of 500 modes always seems to have more even intensity distribution than the upper row. For each total mode number group, the speckle grains are much smaller and clearer to see in the patterns dominated by higher order modes than those in the lower order modes dominated ones. The generated patterns indicate that speckle contrast or spatial coherence is strongly dependent on the composition of the modal field, as has been observed in previous experimental results [20]. It is also noted that the difference of intensity scale bar between Fig. 5 and Fig. 4 is the result of light intensity redistribution on the plane since the random phase modulation. The reason that the speckle patterns don't have the same circular shape as the ones in Fig. 4 is that strong random phase modulation uniformly distributed over $[-\pi, \pi]$ is applied here. If the scale range of the random phase is much narrower, the speckle intensity would concentrate more within the core region.

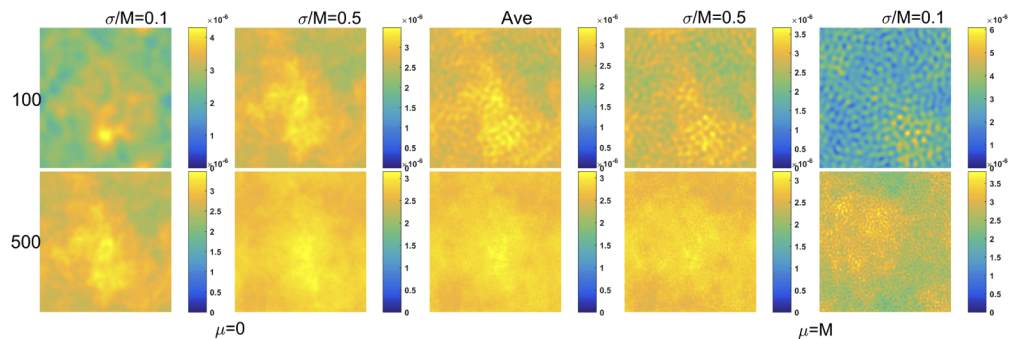


Fig. 5. Calculated speckle patterns formed after light beam passing through the same fixed random phase modulation with different modal composition defined by σ/M for total mode number of 100 (the upper row) and 500 (the lower row). The physical scale is the same with that in Fig. 4. The color bar represents intensity with arbitrary unit.

Using the calculated speckle patterns, quantitative analysis is applied to determine the speckle contrast C . Twenty different random phase matrixes have been used for each modal weight distribution to obtain the average speckle contrast C and its standard deviation value. The calculated C values and their standard deviations for all the cases are shown in Fig. 6. Figure 6 contains three distinctive modal composition regimes. In the left region, μ is zero which means lower order modes dominate. The central region corresponds to uniform distribution regime, while the right region represents $\mu=M$ which means higher order modes are dominating. For each region, five groups of different total mode number ($M=100, 200, 300, 400$ and 500) are evaluated for comparison.

Figure 6 reveals several features. First, starting from the lower order modes dominated case ($\mu=0$) like $\sigma/M=0.1$, when modal weight transfers from the lower order to the higher order modes (i.e., σ/M changes from 0.1 to 0.5), speckle contrast keeps reducing. This demonstrates that the power increase in the higher order modes excites more effective spatial modes that contribute to the reduction of speckle contrast. It is in line with previous knowledge that speckle contrast C is inversely proportional to $\sqrt{M_{eff}}$ (M_{eff} denotes the number of effective spatial modes which have a positive role in the decoherence process). Under this condition, the more effective spatial modes are excited, the lower the speckle contrast would be. However, the trend is not linearly decreasing and finally approaches a minimum value at around $\sigma/M=0.6$. When the power further transfers

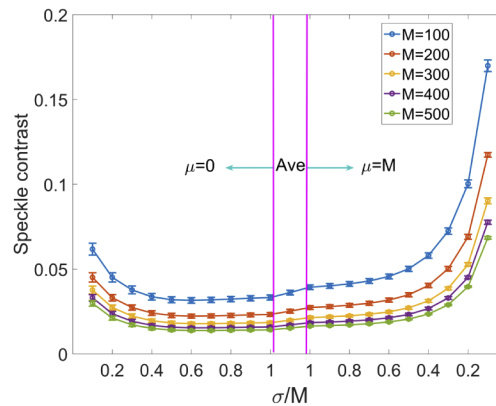


Fig. 6. Calculated average speckle contrast and standard deviation for different modal compositions regimes with different total mode number M .

to higher order modes, the speckle contrast starts to slightly increase (from $\sigma/M=0.7$ to 1, with $\mu=0$). For the central region, when all the modal weight is totally equal, the speckle contrast under this regime is slightly larger than the minimum value of C . For the right region where higher order modes are dominating, the speckle contrast increases rapidly with power further transferring to higher order modes, as shown from $\sigma/M=1$ to 0.1 when $\mu=M$. Therefore, it can be concluded that although the speckle contrast is determined by effective spatial mode number M_{eff} , the M_{eff} is also strongly dependent on the power weight distribution of all the considered spatial eigenmodes. The standard deviation values of the speckle contrast for each case also have similar trends as the average speckle contrast, since more even speckle intensity distribution also leads to lower standard deviation value.

On the other hand, in Fig. 6, for each individual σ/M value, no matter in the right, central or left region, the average speckle contrast is always lower for cases that have larger total mode numbers. This indicates that with the same modal weight distribution the increase of total mode numbers helps to achieve a lower speckle contrast. However, with the increase of total mode number (from $M=100$ to $M=500$), the reduction rate of the speckle contrast seems to slow down, as shown in Fig. 6. This means by unilaterally increasing the total mode number (without increasing the numerical aperture and the length of the MMF, or using much broader bandwidth light), the contribution of newly excited higher order modes on speckle contrast reduction would be weaker than that of the lower order modes.

For the symmetrical modal weight distribution with same σ/M value, but different mean value μ ($\mu=0$ and $\mu=M$), the higher order modes dominated regimes have much higher speckle contrasts, as compared in the right and left regions of Fig. 6. In this regime, the modal composition has much more notable effect on the speckle formation compared to the impact of the number of the effective modes M_{eff} . The more power concentrated in the higher order modes, the larger the speckle contrast C value would be.

All the above results show that lower and higher order spatial eigenmodes have a disparate impact on the speckle formation. Therefore, we investigate the contribution of each of the spatial eigenmodes separately to reveal the intrinsic differences. Each spatial mode is normalized and then modulated by five different random phases. From the five different randomly generated speckle patterns we obtain their corresponding speckle contrasts. All the calculated speckle contrasts for each spatial eigenmode are shown in Fig. 7 depicted by dots with different colors. Four representative speckle patterns corresponding to the 1st, 50th, 200th and 500th order spatial eigenmodes modulated by the same random phase are also shown in the insets of Fig. 7. It is shown that lower order spatial eigenmodes (especially for the first 50 spatial modes) lead to

visibly lower speckle contrasts. When the order of the eigenmode increases, the corresponding speckle contrast becomes larger. Thus, the higher order spatial modes are more conducive to speckle formation, and any power in these modes would lead to higher speckle contrast.

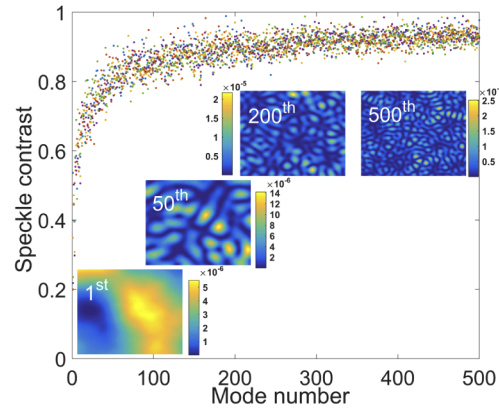


Fig. 7. Calculated speckle contrasts for each normalized spatial eigenmode modulated by five different random phases, where each color of the dots represents an individual random phase. Inset, speckle patterns corresponding to the 1st, 50th, 200th and 500th order spatial eigenmodes. The physical scale is the same with that in Fig. 4. The color bar represents intensity with arbitrary unit.

The unequal contribution of different order spatial eigenmodes is also illustrated by analysis of only two-modes composition regime. Modes that are neighboring (1st and 2nd), or with moderate separation (1st and 50th), or with large separation (1st and 500th, 50th and 500th) with each other are investigated. The corresponding average speckle contrast and standard deviation are shown in Fig. 8. It is worth mentioning that 1000 different random phases are considered here to ensure the rigor of statistical analysis. The modal weight for the lower and higher order mode is represented by w_1 and w_2 respectively. With the value of $(w_2 - w_1)/(w_1 + w_2)$ changing from -1 to 0 to 1, it represents the cases when: (i) only lower order mode is excited, (ii) two modes with equal modal weight are excited and (iii) only higher order mode exists. The dependences reflect the main characteristics observed in Fig. 6. The composition of even only two modes helps to reduce the speckle contrast and the cases with lower order spatial eigenmodes lead to smaller speckle contrast. The minimum value of speckle contrast occurs in the lower order modes dominated regime. The observations found from analysis of a large number of modes in Fig. 6 and the only two-mode composition in Fig. 8, both confirm the fact that lower and higher order modes show evident unequal contributions to spatial coherence and the subsequent impact on speckle formation. Therefore, by controlling the number of excited spatial eigenmodes and the modal weight distribution for lower and higher order modes, the collective spatial coherence can be flexibly tailored.

2.3. Experimental results and discussions

Till now, the remaining question is how to physically implement such tailoring of spatial coherence in MMF. From the above simulation results we can see that the crucial issue is how to effectively transfer the energy from the lower order modes to the higher order ones. However, it is quite challenging to precisely control the modal power distribution of all the considered modes in an individual profile. It has been verified experimentally that more effective spatial eigenmodes can be excited with the increasing of the laser's power [29]. Here, qualitative mode power transfer between the lower and higher order modes is implemented through radially exerted stress on

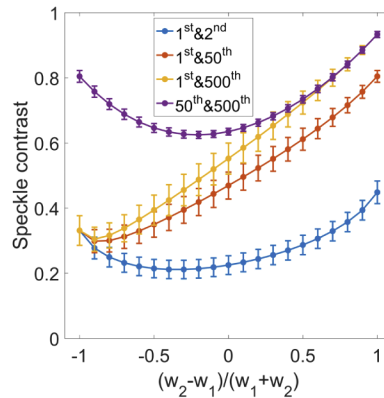


Fig. 8. Calculated average speckle contrasts and standard deviations for two spatial eigenmode compositions (the 1st and 2nd, 1st and 50th, 1st and 500th, 50th and 500th order modes) with different modal weights. 1000 different random phases are considered here.

the MMF, as shown in Fig. 9(a). The output fiber end of a single mode fiber (SMF) based narrow linewidth laser (NLL, central wavelength at 1550 nm, the 3 dB bandwidth is smaller than 0.01 nm) is fusion spliced with a 30 cm length MMF. The output is collimated by a lens with focal length of 6.2 mm. At the input part of the MMF, the stress is exerted by adding weights (stepped by 100 g) on the fiber. It is worth noting that by radially exerting stress on the MMF, the total injected laser power keeps unchanged comparing with our previous approach [29] and the output power of the MMF is also experimentally verified to be unchanged, which means no evident attenuation is induced to the light propagating here. In this way, only the variation of modal power distribution affects the output and the characteristics of spatial coherence. It is anticipated that with the increase of the added weights, lower order spatial eigenmodes keep transferring their energy to the higher order ones.

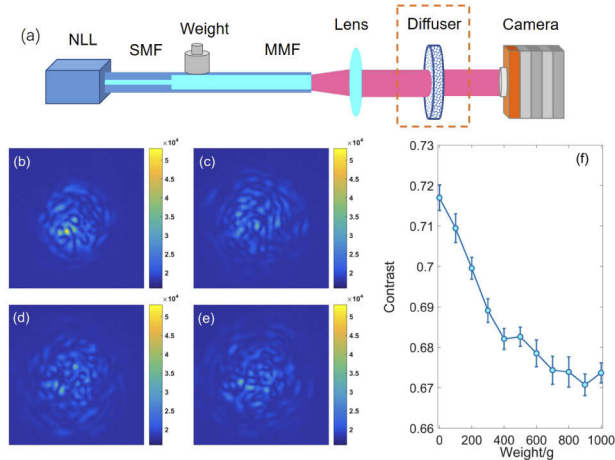


Fig. 9. (a) Experimental diagram of stress induced mode transition. NLL, narrow linewidth laser; SMF, single mode fiber; MMF, multimode fiber. The diffuser in the dashed rectangle is removed when measuring the output mode profile of the MMF. The output mode profiles of the MMF without (b), and with 300 g (c), 600 g (d) and 1000 g (e) weights exerted radially at the input part of the 30 cm length MMF. The color bar represents intensity with arbitrary unit. (f) Measured speckle contrast and its standard deviation for different exerted weights.

Representative mode profiles from the output port of the MMF with different weights are shown in Figs. 9(b)–9(e), which are captured by a near infrared camera (Xenics, Bobcat-640-GigE). With the weights exerted on the MMF, the intensity keeps spreading from the central region (where the lower order spatial eigenmodes concentrate) to the outer region (where the higher order spatial eigenmodes concentrate) and the laser speckle grains become smaller, which verifies the energy transfers from the lower order spatial eigenmodes to the higher order ones. A ground glass diffuser is then inserted before the infrared camera to provide random phase modulation to the output beam from the MMF. Speckle patterns with twenty different random phase states are recorded by the camera to calculate the speckle contrast. The measured speckle contrast and its standard deviation for different exerted weights are shown in Fig. 9(f). The speckle contrast (spatial coherence) keeps reducing with the increasing of the exerted weights, which means more effective spatial modes are excited. These results also coincide well with the left region in Fig. 6 ($\mu=0$), where lower order spatial eigenmodes are dominated. The different values of the measured speckle contrast and the simulated one as shown in Fig. 6 is caused by both the limited number of excited spatial eigenmodes since SMF light is preferable to excite lower order spatial modes and the short MMF length which means not all the excited high order spatial modes are completely decoherent with the limited accumulated group velocity dispersion. However, it is not likely to further transfer the lower order modes into higher order ones, since the initial coupling of light injecting into the MMF is fusion spliced with axial alignment. Prior excitation of the lower order spatial eigenmodes is expected for this considered input coupling. The higher order modes dominated regime could be obtained by increasing the angle of the incident light if free-space coupling is used. Offset light coupling injection could also be a potential method to preferentially excite higher order spatial eigenmodes. Other effective methods to precisely excite different groups of spatial eigenmodes are of great interest for future research.

3. Conclusion

In this paper, we studied the effect of the unequal contribution of lower and higher order modes on speckle formation. We found that higher order spatial modes are prone to generate more severe speckles. The transverse mode profile of individual modes should be taken into consideration when analyzing its impact on speckle formation or spatial coherence of the light beam. The lowest speckle contrast is a trade-off between the number of effective transverse modes and the modal weight distribution. Therefore, increasing the number of transverse modes could lead to lower speckle contrast. However, at the same time, the modal weight distribution should be more even to excite more effective transverse modes. Our results offer a glimpse of the way to customize the spatial coherence of light by selectively exciting groups of eigenmodes theoretically. However, the practical realization of such an individual modal power distribution for different order of spatial eigenmodes still needs further study. These results unveil the intrinsic unequal contribution of the lower and higher transverse modes to speckle formation and spatial coherence, which could help in optimization of tailoring the spatial coherence of the fiber output field and help to design light sources with a spatial coherence on demand.

Funding

National Natural Science Foundation of China (11974071, 61635005, 61811530062); China Scholarship Council (201806070008); Russian Science Foundation (17-72-30006).

Disclosures

The authors declare no conflicts of interest.

References

1. J. W. Goodman, "Speckle Phenomena in Optics: Theory and Applications," Roberts & Company, Englewood (2007).
2. J. D. Briers, "Laser Doppler, speckle and related techniques for blood perfusion mapping and imaging," *Physiol. Meas.* **22**(4), R35–R66 (2001).
3. D. A. Boas and A. K. Dunn, "Laser speckle contrast imaging in biomedical optics," *J. Biomed. Opt.* **15**(1), 011109 (2010).
4. Y. C. Shih, A. Davis, S. W. Hasinoff, F. Durand, and W. T. Freeman, "Laser speckle photography for surface tampering detection," *Proceedings of the 2012 IEEE Conference on Computer Vision and Pattern Recognition*, 33–40 (2012).
5. B. Redding, M. A. Choma, and H. Cao, "Speckle-free laser imaging using random laser illumination," *Nat. Photonics* **6**(6), 355–359 (2012).
6. F. Wang, X. Liu, Y. Yuan, and Y. Cai, "Experimental generation of partially coherent beams with different complex degrees of coherence," *Opt. Lett.* **38**(11), 1814–1816 (2013).
7. M. Nixon, B. Redding, A. A. Friesem, H. Cao, and N. Davidson, "Efficient method for controlling the spatial coherence of a laser," *Opt. Lett.* **38**(19), 3858–3861 (2013).
8. H. Farrokhi, T. M. Rohith, J. Boonruangkan, S. Han, H. Kim, S. W. Kim, and Y. J. Kim, "High-brightness laser imaging with tunable speckle reduction enabled by electroactive micro-optic diffusers," *Sci. Rep.* **7**(1), 15318 (2017).
9. D. S. Mehta, D. N. Naik, R. K. Singh, and M. Takeda, "Laser speckle reduction by multimode optical fiber bundle with combined temporal, spatial, and angular diversity," *Appl. Opt.* **51**(12), 1894–1904 (2012).
10. J. G. Manni and J. W. Goodman, "Versatile method for achieving 1% speckle contrast in large-venue laser projection displays using a stationary multimode optical fiber," *Opt. Express* **20**(10), 11288–11315 (2012).
11. B. Redding, P. Ahmadi, V. Mokan, M. Seifert, M. A. Choma, and H. Cao, "Low-spatial-coherence high-radiance broadband fiber source for speckle free imaging," *Opt. Lett.* **40**(20), 4607–4610 (2015).
12. J. Carpenter, B. J. Eggleton, and J. Schröder, "Observation of Eisenbud–Wigner–Smith states as principal modes in multimode fibre," *Nat. Photonics* **9**(11), 751–757 (2015).
13. M. Plöschner, T. Tyc, and T. Čížmár, "Seeing through chaos in multimode fibres," *Nat. Photonics* **9**(8), 529–535 (2015).
14. L. G. Wright, Z. Liu, D. A. Nolan, M. Li, D. N. Christodoulides, and F. W. Wise, "Self-organized instability in graded-index multimode fibres," *Nat. Photonics* **10**(12), 771–776 (2016).
15. K. Krupa, A. Tonello, B. M. Shalaby, M. Fabert, A. Barthélémy, G. Millot, S. Wabnitz, and V. Couderc, "Spatial beam self-cleaning in multimode fibres," *Nat. Photonics* **11**(4), 237–241 (2017).
16. E. V. Podivilov, D. S. Kharenko, V. A. Gonta, K. Krupa, O. S. Sidelnikov, S. Turitsyn, M. P. Fedoruk, S. A. Babin, and S. Wabnitz, "Hydrodynamic 2D Turbulence and Spatial Beam Condensation in Multimode Optical Fibers," *Phys. Rev. Lett.* **122**(10), 103902 (2019).
17. A. Efimov, "Spatial coherence at the output of multimode optical fibers," *Opt. Express* **22**(13), 15577–15588 (2014).
18. A. Efimov, "Coherence and speckle contrast at the output of a stationary multimode optical fiber," *Opt. Lett.* **43**(19), 4767–4770 (2018).
19. R. Ma, Y. J. Rao, W. L. Zhang, and B. Hu, "Multimode random fiber laser for speckle-free imaging," *IEEE J. Sel. Top. Quantum Electron.* **25**, 1 (2019).
20. R. Ma, W. L. Zhang, J. Y. Guo, and Y. J. Rao, "Decoherence of fiber supercontinuum light source for speckle-free imaging," *Opt. Express* **26**(20), 26758–26765 (2018).
21. T. H. Wood, "Actual modal power distributions in multimode optical fibers and their effect on modal noise," *Opt. Lett.* **9**(3), 102–104 (1984).
22. T. H. Wood and L. A. Ewell, "Increased received power and decreased modal noise by preferential excitation of low-order modes in multimode optical-fiber transmission systems," *J. Lightwave Technol.* **4**(4), 391–395 (1986).
23. J. Saijonmaa and S. J. Halme, "Reduction of modal noise by using reduced spot excitation," *Appl. Opt.* **20**(24), 4302–4306 (1981).
24. T. Kaiser, D. Flamm, and M. Duparré, "Complete modal decomposition for optical fibers using CGH-based correlation filters," *Opt. Express* **17**(11), 9347–9356 (2009).
25. A. B. Fallahkhair, K. S. Li, and T. E. Murphy, "Vector finite difference modesolver for anisotropic dielectric waveguides," *J. Lightwave Technol.* **26**(11), 1423–1431 (2008).
26. [Online]. Available: <https://photonics.umd.edu/software/wgmodes/>
27. L. Pan, X. Chao, Z.-C. Ren, H.-T. Wang, and J. Ding, "Measuring spatial coherence by using a lateral shearing interferometry," *Appl. Opt.* **58**(1), 56–61 (2019).
28. C. Koebele, M. Salsi, D. Sperti, P. Tran, P. Brindel, H. Mardoyan, S. Bigo, A. Boutin, F. Verluise, P. Sillard, M. Astruc, L. Provost, F. Cerou, and G. Charlet, "Two mode transmission at 2 (100Gb/s, over 40km-long prototype few-mode fiber, using LCOS-based programmable mode multiplexer and demultiplexer," *Opt. Express* **19**(17), 16593–16600 (2011).
29. R. Ma, J. Q. Li, J. Y. Guo, H. Wu, H. H. Zhang, B. Hu, Y. J. Rao, and W. L. Zhang, "High-power low spatial coherence random fiber laser," *Opt. Express* **27**(6), 8738–8744 (2019).